J. Fluid Mech. (1992), *vol.* 245, *pp.* 493–521

Test flow disturbances in an expansion tube

By A. PAULL AND R. J. STALKER
Mechanical Engineering Department, University of Queensland, Brisbane, Qld 4072, Australia

(Received 3 July 1991 and in revised form 28 May 1992)

The operation of an expansion tube is investigated with particular attention given to the test flow disturbances which have limited their utility in the past. Theoretical bounds for the duration of uniform test flow are first explored using one-dimensional ideal-gas relations, together with shock-tube boundary-layer entrainment effects. It is seen that test flow duration is limited either by the arrival of the downstream edge of the test-gas unsteady expansion or by the arrival of the upstream edge of this expansion after it has been reflected from the driver–test gas interface. These bounds are seen to be in good agreement with measurements made with large driver-gas expansion ratios. For small expansion ratios additional disturbances are observed in the test gas. Similar disturbances are also observed in the driver gas. It is postulated that these disturbances first appear in the driver gas and are transmitted into the test gas before the test gas is expanded. These disturbances remain with the test gas as it is expanded and subsequently produce unsteady conditions at the test section. Theoretical calculations for the range of frequencies which occur in the test gas before the expansion are obtained by modelling the disturbances as acoustic waves. It is shown that only the high-frequency components of the disturbances in the driver gas can penetrate the driver–test gas interface and this provides a mechanism for suppressing disturbances in the test gas. Additional analytical calculations for the shift in frequency produced as an acoustic wave traverses an unsteady expansion are also presented and it is shown that all frequencies of a given acoustic wave mode converge to one frequency. This focusing of frequencies is seen to occur in three different facilities.

1. Introduction

An expansion tube is an impulse hypersonic facility which can produce high-enthalpy quasi-steady flows. In comparison with the more widely used reflected shock tunnel, expansion tubes offer substantial gains in both stagnation enthalpy and effective stagnation pressure together with a decrease in free-stream dissociation levels. These advantages are obtained because the expansion tube accelerates the test gas through an unsteady expansion, whereas the reflected shock tunnel utilizes a steady expansion through a supersonic nozzle.

The potential of the expansion tube as a device for generating hypersonic flows was pointed out by Trimpi (1962), who predicted theoretically that it could access a large range of test conditions. Following this analysis, a number of expansion tubes were constructed and assessed experimentally (Norfleet, Lacey & Whitfield 1965; Spurk 1965) with generally disappointing results. The anticipated test times were not realized in practice, largely due to the unexpected appearance of high-frequency disturbances in the test flow. An exception was the expansion tube described by Miller (1977) where a narrow window of acceptably steady test conditions was obtained for each test gas.

The analysis presented here explores the reasons for the past failure of the expansion tube to realize its theoretical expectations. It explains why the window of steady test conditions is small and indicates how this window can be widened so that these facilities could be used in a variety of hypersonic research. In addition to the theoretical results, centreline Pitot pressure measurements obtained with air as test gas, are also presented to experimentally confirm theoretical predictions.

2. Summary of theoretical development

An expansion tube consists of three consecutive sections; the driver tube, the shock tube and the acceleration tube, as indicated in figure 1. The acceleration tube empties unrestrictively into a dumptank test section. These three sections are initially filled with the driver, test and acceleration gases, respectively.

Initially the three sections are separated by two diaphragms. The heavier of these is the primary diaphragm which is between the driver and shock tubes, while the shock and acceleration tubes are initially separated by the secondary diaphragm. Ideally, the secondary diaphragm is massless. For the gas densities used in the experiments reported here a massless diaphragm is a good approximation.

An expansion tube is operated by initially raising the pressure in the driver tube so that the primary diaphragm ruptures. This produces a shock which travels through the test gas towards the secondary diaphragm. For a massless secondary diaphragm the shock ruptures this diaphragm without reflecting, instantaneously accelerates, then travels down the acceleration tube with constant velocity. The test gas follows the shock and accelerates through an unsteady expansion centred at the secondary diaphragm. The test time is the period of steady flow following the arrival of the test–acceleration gas interface at the test section, as shown in figure 2.

The performance of an expansion tube is measured in terms of the flow properties of the test gas at the test section and the time over which the flow is steady. It is influenced by twelve independent parameters, namely the lengths and diameters of the driver, shock and acceleration tubes, the gases which initially reside in these tubes and the initial filling pressures.

In practice, the internal diameters of the shock and acceleration tubes and the geometry of the driver tube are fixed after they have been manufactured. Thus, the number of independent parameters which may be varied is reduced to eight. This is still a large number and it is this large number of degrees of apparatus freedom which makes it difficult to readily acquire an understanding of the performance characteristics of an expansion tube.

2.1. *Test time limitations*

There are two distinct ranges of flow conditions in which different mechanisms limit the test time. These flow regimes will be referred to as the high-enthalpy conditions and the low-enthalpy conditions. To a good approximation, the high- and low-enthalpy conditions are generated when the driver-gas sound speed at the driver–test gas interface in the shock tube is respectively less than and greater than the test-gas sound speed. This approximation becomes less valid as the diameter of the expansion tube is increased and as the driver-gas sound speed prior to rupturing the primary diaphragm is decreased.

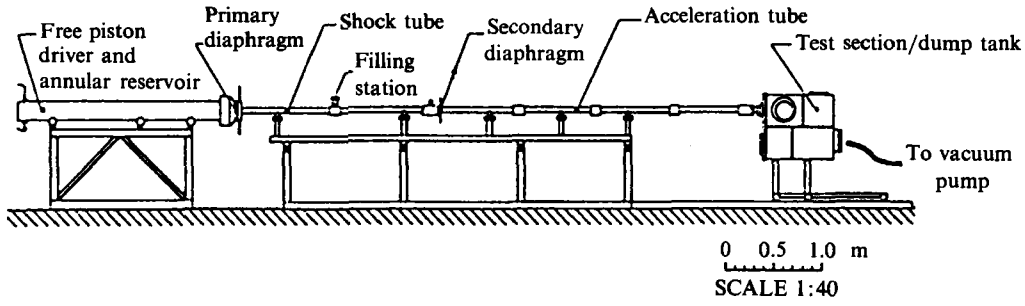

FIGURE 1. Schematic of an expansion tube.

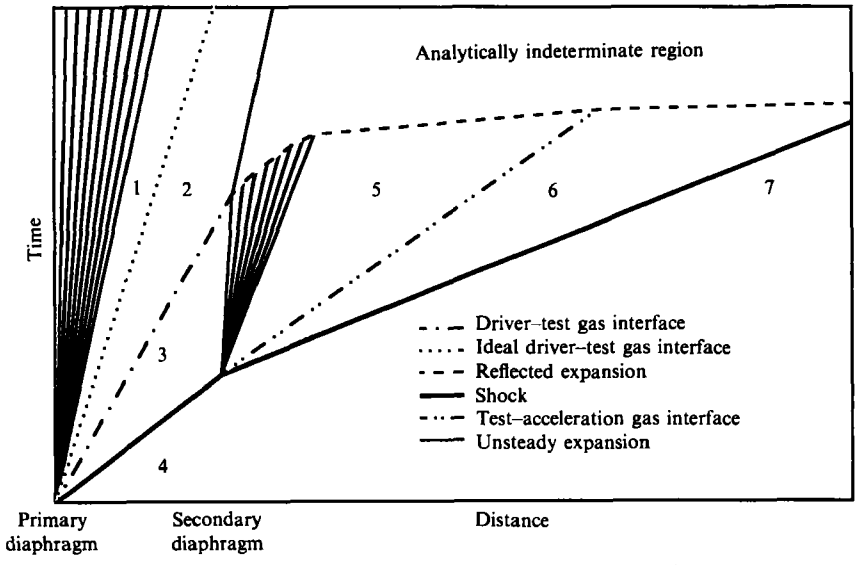

FIGURE 2. X–t diagram for an expansion tube.

2.1.1. *High-enthalpy conditions*

High-enthalpy conditions are obtained by using a shock-tube filling pressure which is sufficiently low that the driver-gas sound speed decreases across the expansion centred at the primary diaphragm to a value which is less than that of the test gas at the interface. At high-enthalpy conditions a test time may be predicted using ideal inviscid one-dimensional gas dynamics as indicated by Trimpi (1962). Trimpi's analysis assumes that the test time is limited by the arrival at the test section of the unsteady expansion generated when the secondary diaphragm ruptures. It can be seen from figure 2 that this is only correct if the acceleration tube is sufficiently short that the reflection of the unsteady expansion off the driver–test gas interface arrives at the test section after the downstream edge of the unsteady expansion.

Trimpi's analysis assumes that the location of the driver–test gas interface can be predicted using ideal inviscid one-dimensional gas dynamics. If this assumption were correct this interface would be sufficiently far upstream that the reflection of the unsteady expansion would not normally limit the test time. However, Mirels (1964) has shown that the boundary layer entrains mass and acts like a mass sink. This

significantly decreases the distance between the shock and the interface in the shock tube. Hence, the unsteady expansion produced when the secondary diaphragm ruptures can reflect off the driver–test gas interface and arrive at the test section before the downstream edge of the unsteady expansion.

The analysis presented here predicts the location of the driver–test gas interface using Mirels' theory and then analytically determines the trajectory of the downstream edge of the reflected expansion. The analysis also obtains Trimpi's (1962) result for the trajectory of the downstream edge of the expansion before the reflected expansion arrives at this edge. These two trajectories are then used to predict the available test times. It is shown experimentally that this prediction of the available test time is good for high-enthalpy conditions.

2.1.2. *Low-enthalpy conditions*

In general, at low-enthalpy conditions the theoretical assessment applicable to high-enthalpy conditions is insufficient. At low-enthalpy conditions during the steady test period predicted by the above analysis, it is found that the test flow can be rendered unacceptably noisy by high-frequency fluctuations in observables such as the Pitot pressure. It is argued here that the dominant part of this noise can be modelled as acoustic lateral waves which are generated in the driver gas. These waves are transmitted through the driver–test gas interface into the test gas before the secondary diaphragm ruptures.

It is important to recognize that the mechanisms for generating this noise are also present for the high-enthalpy conditions. The noise is not transmitted through the interface at the high-enthalpy conditions because the test-gas sound speed is greater than the driver-gas sound speed. For this mismatch of sound speeds it will be shown that the interface acts as a low-frequency filter and totally reflects low-frequency lateral waves.

Although not all of the noise sources observed in the driver gas have been positively identified, it will be shown that a significant portion can be attributed to noise generated in the primary-diaphragm rupturing process. Furthermore, the filtering of this diaphragm noise is sufficient to produce acceptable test conditions.

2.2. *Frequency focusing*

A further process which disrupts the test time is produced when the unsteady expansion centred at the secondary diaphragm produces a large drop in the sound speed of the test gas. It has been shown by Paull & Stalker (1991) that all frequency components of noise transmitted through the expansion will be 'focused' into a narrow bandwidth of frequencies. This results in a pronounced disturbance downstream of the expansion and thus the test flow is rendered useless. Frequency focusing is discussed here in more detail and in the context of the more general theory. In addition, frequency focusing is used to confirm the existence of lateral waves in the test gas.

The effects produced by frequency focusing generally only disrupt the test flow at the low-enthalpy conditions. This is because at the high-enthalpy conditions the test gas is relatively quiet prior to the secondary diaphragm rupturing. Hence, although focusing will occur, the amplitude of the noise is reduced to an acceptable level.

3. Experimental apparatus

Figure 1 is a diagrammatic representation of the expansion tube used in the experiments reported here. It is identical to that described by Neely, Stalker & Paull (1991). It incorporates a free piston driver (Stalker 1966) in the driver tube to increase the driver-gas pressure sufficiently to rupture the primary diaphragm.

The inside diameter of the driver tube was 100 mm and the inside diameters of the shock and acceleration tubes were 37 m. The length of the shock and acceleration tubes were 2.08 m and 3.18 m respectively. These lengths were not changeable.

Pitot pressure measurements were taken on the centreline at the exit of the acceleration tube. The wall pressure was measured 14 mm upstream of the exit of the acceleration tube. The Pitot pressure involved a transducer mounted to measure the pressure in a cavity which faced upstream into the oncoming flow. Estimates indicate that the natural frequency of this cavity exceeded 100 kHz. This was confirmed by observing that the rise time of the pressure in the cavity, in response to an impinging shock, was less than 5 μs. All quantities were sampled every microsecond.

4. Test time at high-enthalpy conditions

At high-enthalpy conditions the test time will be limited by either the downstream edge of the unsteady expansion centred at the secondary diaphragm rupture or the downstream edge of the reflection of the upstream edge of this expansion off the driver–test gas interface, as seen in figure 2. The theoretical test time is obtained by assuming inviscid, one-dimensional flow of a perfect gas in all calculations except that which determines the location of the driver–test gas interface. This is obtained using Mirels' (1964) ideal gas theory for boundary-layer entrainment.

For a one-dimensional inviscid flow of a perfect gas

$$u \pm 2/(\gamma-1)\,a = \text{const.}, \tag{4.1a, b}$$

along the characteristics

$$\mathrm{d}x/\mathrm{d}t = u \pm a, \tag{4.2a, b}$$

where u is the gas velocity, a is the local sound speed and γ is the specific heat ratio. It follows (Whitham 1974, pp. 157, 158) that within a centred unsteady expansion

$$u = \frac{\gamma-1}{\gamma+1}u_3 + \frac{2}{\gamma+1}\left(a_3 + \frac{x}{t}\right), \tag{4.3}$$

and

$$a = \frac{2}{\gamma+1}a_3 + \frac{\gamma-1}{\gamma+1}\left(u_3 - \frac{x}{t}\right), \tag{4.4}$$

where subscript 3 refers to the conditions upstream of the expansion as seen in figure 2. The origin in (4.3) and (4.4) of the (x, t)-space is at the rupture of the secondary diaphragm.

4.1. *Test time bounds*

If the test time is limited by the downstream edge of the unsteady expansion then the test time, T, is the time elapsed between the arrival of the test–acceleration gas interface and this edge, as seen in figure 2. This interface and edge have velocities u_5 and $u_5 - a_5$ respectively, where subscript 5 refers to the test-gas conditions downstream of the expansion. Hence, the test time is

$$T = \frac{x_{\mathrm{A}}\, a_5}{u_5(u_5 - a_5)}, \tag{4.5}$$

where x_{A} is the length of the acceleration tube.

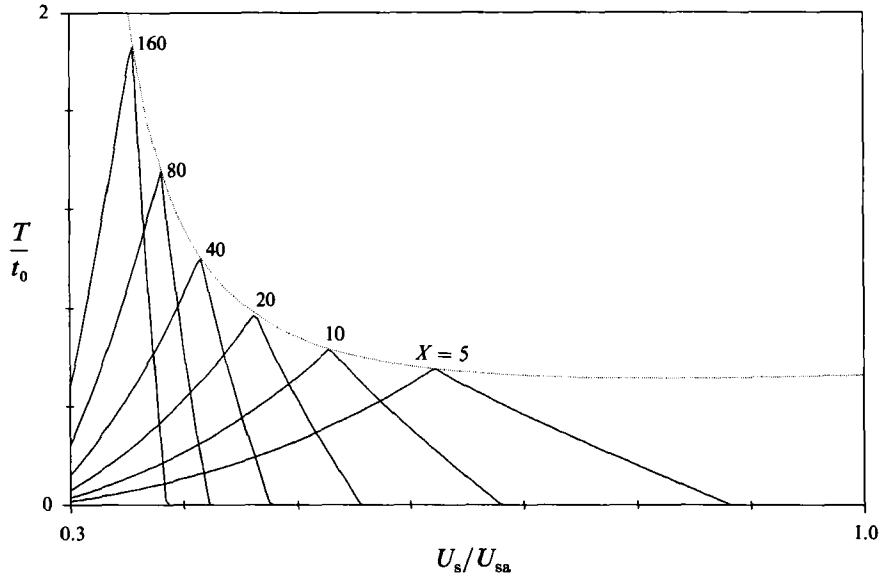

FIGURE 3. Non-dimensional test time for different non-dimensional acceleration tube lengths as a function of the ratio of shock speeds in the shock and acceleration tubes for strong shocks with $\gamma = \frac{7}{5}$.

If the test time is limited by the reflected expansion then the test time is determined analytically as a function of the elapse time, t_0, between rupture of the secondary diaphragm and arrival of the driver–test gas interface at the upstream edge of the unsteady expansion. Within the expansion the characteristic curve which marks the downstream edge of the reflected expansion is obtained analytically from integration of (4.2a) with u and a given by (4.3) and (4.4), respectively. The intersection of this trajectory and the trajectory of the downstream edge of the expansion determines the time for the downstream edge of the reflected expansion to emerge from the expansion. The time elapsed between this event and rupturing of the secondary diaphragm is

$$t_1 = t_0(a_5/a_3)^{\frac{\gamma+1}{2(1-\gamma)}}. \tag{4.6}$$

The downstream edge of the reflected expansion then travels in the uniform flow ahead of the expansion with constant velocity $u_5 + a_5$ until it reaches the test section or the test–acceleration interface. In the latter case there is no test time; otherwise the test time is

$$T = \frac{a_5}{u_5 + a_5}\left(2t_1 - \frac{x_A}{u_5}\right). \tag{4.7}$$

It can be seen from (4.1a), which relates conditions either side of the expansion, (4.6) and (4.7) that the non-dimensional test time, T/t_0, is a function of the sound speed ratio a_5/a_3 and the non-dimensional acceleration-tube length $X = x_A/(a_3 t_0)$. The non-dimensional acceleration-tube length is the ratio of acceleration-tube length to the effective inviscid test-gas slug length in the shock tube when the secondary diaphragm ruptures. For strong shocks it follows that this non-dimensional test time is approximately a function of the shock speed ratio U_{sa}/U_s and the non-dimensional acceleration tube length, where U_{sa} and U_s are the shock speeds in the acceleration and shock tubes respectively.

Figure 3 displays the non-dimensional test time as a function of shock speed ratio for different non-dimensional acceleration tube lengths and a specific heat ratio of $\frac{7}{5}$.

In the regions where the test time is monotonically increasing with U_s/U_{sa} the test time is limited by the downstream edge of the unsteady expansion and is determined from (4.5). When the test time is monotonically decreasing with U_s/U_{sa} the test time is limited by the reflected unsteady expansion and is determined from (4.6) and (4.7).

4.2. *Maximum test time*

It can be seen that the reflected expansion severely limits the available test time. Hence, if a facility is to have the largest possible window of test conditions then the length of the acceleration tube must not be fixed. It should be adjusted for each condition so that the test time is maximized.

From inspection of figures 2 and 3 it can be seen that the maximum available test time is obtained when the reflected expansion and the unsteady expansion arrive at the test section simultaneously. The maximum test time is indicated by the dotted line in figure 3. By equating (4.5) and (4.7) it can be shown that the maximum test time is

$$T_m = (t_0/M_5)\,(a_3/a_5)^{\frac{\gamma+1}{2(\gamma-1)}}, \tag{4.8}$$

where $M_5 = u_5/a_5$ is the local Mach number of the test gas. From the substitution of (4.8) for T in (4.5) it follows that this maximum test time is achieved if the non-dimensional length of the acceleration tube is

$$X = (M_5 - 1)\,(a_3/a_5)^{\frac{3-\gamma}{2(\gamma-1)}}. \tag{4.9}$$

Hence, to obtain the best performance from an expansion tube the filling pressures and acceleration tube length must be chosen so that (4.9) is satisfied.

4.3. *Estimation of* t_0

In all the experiments reported here Mirels' (1964) turbulent boundary-layer analysis for an ideal gas and strong shocks has been used to determine the location and velocity of the driver–test gas interface. This analysis indicates that turbulent boundary-layer theory is required if $P_4 r_0 > 0.085$ m kPa (where r_0 is the tube radius). In the experiments reported here $P_4 > 0.062$ m kPa. Hence, although some experiments are in the transitional region the majority should have turbulent boundary layers.

The elapse time t_0 between rupture of the secondary diaphragm and the arrival of the interface at the upstream edge of the unsteady expansion is determined by assuming that the interface travels with constant velocity u_i after the diaphragm ruptures. The position of the upstream edge of the unsteady expansion is obtained as a function of time from the characteristic equation (4.2*b*). It is assumed that after the diaphragm ruptures the gas velocity between the shock and the interface varies linearly with distance. This approximation is made to obtain a simple analytical relationship between t_0 and the properties of the gas behind the shock. A more accurate method would be to use the gas velocity provided by Mirels (1964). For this linear approximation the gas velocity encountered by the upstream edge of the expansion is

$$u = \frac{u_i - u_{30}}{l}(x_i - x) + u_i, \tag{4.10}$$

where l is the separation of the shock and interface when the diaphragm ruptures, x_i is the position of the interface relative to an origin located at the diaphragm, u_{30} is the gas velocity immediately after the primary shock and u_i is the interface velocity.

The positive x-direction is in the flow direction. The values of u_i and l are obtained using Mirels' (1964) theory for boundary-layer entrainment.

If the interface travels with constant velocity then

$$x_i = u_i t - l. \tag{4.11}$$

The substitution of (4.11) into (4.10) gives the gas velocity upstream of the expansion as a function of position and time. If it is also assumed that the sound speed is constant and equal to a_3 then an estimate of the trajectory of the upstream edge of the unsteady expansion is obtained from the integration of the characteristic equation (4.2*b*) with the velocity given by (4.10). The intersection of this curve and the straight line (4.11) gives an estimate of the elapse time t_0 of

$$t_0 = \frac{l}{u_i - u_{30}} \ln\left(\frac{a_3 + u_i - u_{30}}{a_3}\right). \tag{4.12}$$

5. Acoustic wave theory

It will be shown in §8 that the test times predicted in §4 are accurate only at higher-enthalpy conditions. At lower-enthalpy conditions where the analysis of §4 predicts considerable test time, it has already been noted that the flow is in fact very 'noisy'. This noise will be modelled as acoustic waves which are small perturbations of both velocity and pressure about a steady mean. It will be seen that this model describes the properties of the noise sufficiently to allow its effects to be understood and controlled.

For small perturbations Whitham (1974, pp. 157, 158) shows that the velocity and pressure can be written as

$$\boldsymbol{u} = \boldsymbol{u}_0 + \nabla\phi, \tag{5.1}$$

and

$$p = p_0 - \rho_0 \partial\phi/\partial t, \tag{5.2}$$

respectively, where the potential function ϕ is a solution to the wave equation, $\boldsymbol{u}_0$, p_0 and ρ_0 are the unperturbed steady velocity, pressure and density respectively and t is time.

It will be seen that the noise observed experimentally has properties consistent with those potential functions which are only dependent on time, radial distance r, and axial distance x. These functions have the form

$$\phi = J_0(\lambda r) \exp\left(\mathrm{i}\omega(t \pm \beta x/a)\right), \tag{5.3}$$

where J_0 is the zeroth-order Bessel function of the first kind, a is the local sound speed, ω is the fundamental frequency and the dispersive term is

$$\beta = (1 - (\lambda a/\omega)^2)^{\frac{1}{2}}. \tag{5.4}$$

The spatial origin is fixed in a frame in which the gas is at rest.

The permissible values of λ are obtained by imposing the no-penetration boundary condition,

$$(\partial\phi/\partial r)(r_0, t) = 0, \tag{5.5}$$

at the wall of the expansion tube. It follows that λr_0 is equal to any of the infinite number of discrete zeros of the first-order Bessel function of the first kind, J_1. The first zero of J_1 occurs when λr_0 equals zero. $J_0(0) = 1$, hence from (5.3) this solution is radially independent. Solutions of this form are called longitudinal waves. All other

solutions are radially dependent and will be referred to as lateral waves. For the lowest-order lateral wave $\lambda \approx 3.83/r_0$.

Centreline Pitot pressure measurements are used in §8 to detect the acoustic wave disturbances. Hence, it is important to know how a small perturbation would affect the Pitot pressure measurement. It will be assumed that fluctuations in Pitot pressure, P_T, produced by small disturbances can be determined from Rayleigh's Pitot pressure formula (Liepmann & Roshko 1957)

$$P_T = P_s M^2 (\tfrac{1}{2}(\gamma+1))^{\frac{\gamma+1}{\gamma-1}} (\gamma - \tfrac{1}{2}(\gamma-1) M^{-2})^{\frac{1}{1-\gamma}}, \tag{5.6}$$

where P_s is the static pressure and M is the local Mach number.

From the substitution of (5.1) and (5.2) for the velocity and static pressure in (5.6) it can be shown that, to first order in the derivatives of ϕ,

$$P_T = P_{T_0}\left(1 + \frac{2M_0^2 - 1}{M_0^2 - (\gamma-1)/2\gamma} U_0^{-1} \frac{\partial \phi}{\partial x} - \gamma a^{-2} \frac{\partial \phi}{\partial t}\right), \tag{5.7}$$

where M_0 and P_{T_0} are the unperturbed Mach number and Pitot pressure, respectively. If the potential function is of the form (5.3) then the Pitot pressure can be expressed as

$$P_T = P_{T_0}(1 - i\epsilon(M, a, \beta, \gamma)\phi), \tag{5.8}$$

where

$$\epsilon(M, a, \beta, \gamma) = \omega a^{-2}\left(\gamma \mp \frac{2M_0^2 - 1}{M_0^2 - (\gamma-1)/2\gamma} \frac{\beta}{M_0}\right). \tag{5.9}$$

5.1. *Doppler shifts*

In (5.3), x has its origin fixed in a frame in which the unperturbed gas is at rest. However, in a laboratory the unperturbed gas is in motion relative to the observer. Thus, a Doppler shift in the frequency is observed.

5.1.1. *Doppler shift due to a linear translation*

If the unperturbed gas moves with a constant velocity u relative to the laboratory then the frequency observed in the laboratory is obtained by translating the axial component in (5.3) by ut. It can then be shown from the coefficient of the time variable in the exponent of (5.3) that the frequency observed in the laboratory would be

$$\nu = \omega(1 \mp u\beta/a)/2\pi. \tag{5.10}$$

In the case of a longitudinal wave $\beta = 1$. Hence, the Doppler shift is only dependent upon the local Mach number u/a. In contrast, the form of β ensures that the Doppler shift for lateral waves depends separately on both the sound speed and gas velocity.

5.1.2. *Frequency change across an unsteady expansion – frequency 'focusing'*

When an acoustic wave encounters an unsteady expansion, solutions of the form (5.3) are not directly applicable within the confines of the expansion because the unperturbed state is not steady. However, these acoustic wave solutions can be used to determine the shift in frequency which would be observed as the acoustic wave traverses the expansion. Following the approach used by Godunov (1959) the expansion is divided along the characteristic lines into discrete steady regions and acoustic theory is applied within these regions. Between these regions there is a discontinuity in both sound speed and gas velocity. Furthermore, the discontinuity itself has a velocity which is different to both the gas velocities of its adjacent regions.

Before the shift in frequency across the entire expansion is obtained, the frequency shift across an interface separating two regions which have different sound speeds and gas velocities is determined. To be applicable to subsequent analysis of the entire expansion the interface has a velocity different to the gas velocities in both regions. The velocity of the interface and the gas velocities either side of the interface are constant with time. The two regions will have their properties subscripted by 1 and 2 and it will be assumed that an acoustic wave described by (5.3) is incident in region 1 and is transmitted through the interface into region 2.

The interface is a boundary for region 2 upon which conditions are imposed which uniquely determine the solution to the wave equation in region 2. In the degenerate case when there is no discontinuity in the gas velocities and the interface velocity is the same as the gas velocity, it can be seen by equating the time coefficients in the exponent of (5.3) from either side of the interface that the fundamental frequency is the same in both regions. However, in the more complex situation where there is a discontinuity in the gas velocity this is not the case. The interface is the boundary which drives the solution in region 2; hence, the fundamental frequency in region 2 must be chosen so that it is equal to the frequency which is observed at the interface. That is to say, the frequency as observed in the frame of the interface shall be continuous across the interface. Hence, from (5.10) the fundamental frequencies either side of the interface are related by

$$\omega_1(1+(u_1-v)\beta_1/a_1) = \omega_2(1+(u_2-v)\beta_2/a_2), \tag{5.11}$$

where v is the interface velocity.

The change in frequency across the entire unsteady expansion is now considered. In this more general case the expansion is initially divided into a finite number of regions in which the properties are constant, as described above. The properties of the regions will be subscripted with the letter i. $i = 0$ refers to the steady region upstream of the expansion.

The interface between adjoining regions i and $i+1$ propagates upstream along a characteristic line and therefore has velocity $u_i - a_i$. Hence, from (5.11) the fundamental frequencies either side of the interface are related by

$$\omega_i(1+\beta_i) = \omega_{i+1}(1+(u_{i+1}-u_i+a_i)\beta_{i+1}/a_{i+1}). \tag{5.12}$$

The sound speeds and gas velocities of the two regions are related by (**4.1***a*). Eliminating the velocity terms in (5.12) it follows that

$$\omega_i(1+\beta_i) = \omega_{i+1}\left(1+\left(1-\frac{\gamma+1}{\gamma-1}\frac{\mathrm{d}a_i}{a_{i+1}}\right)\beta_{i+1}\right), \tag{5.13}$$

where $\mathrm{d}a_i = a_{i+1} - a_i$.

The limit in which the number of discrete steady regions approaches infinity and the amplitudes of the discontinuities approach zero is then taken. The resulting equation is combined with a relationship obtained from (5.4) between the infinitesimal change in the fundamental frequency and the infinitesimal changes in the dispersive term and the sound speed. This is done in order to develop a differential relationship between the sound speed and the dispersive term within the expansion, which when integrated gives

$$\frac{\beta-\frac{1}{2}(\gamma-1)}{\beta-1} = \frac{\beta_0-\frac{1}{2}(\gamma-1)}{\beta_0-1}\left(\frac{a}{a_0}\right)^{\frac{3-\gamma}{\gamma-1}}. \tag{5.14}$$

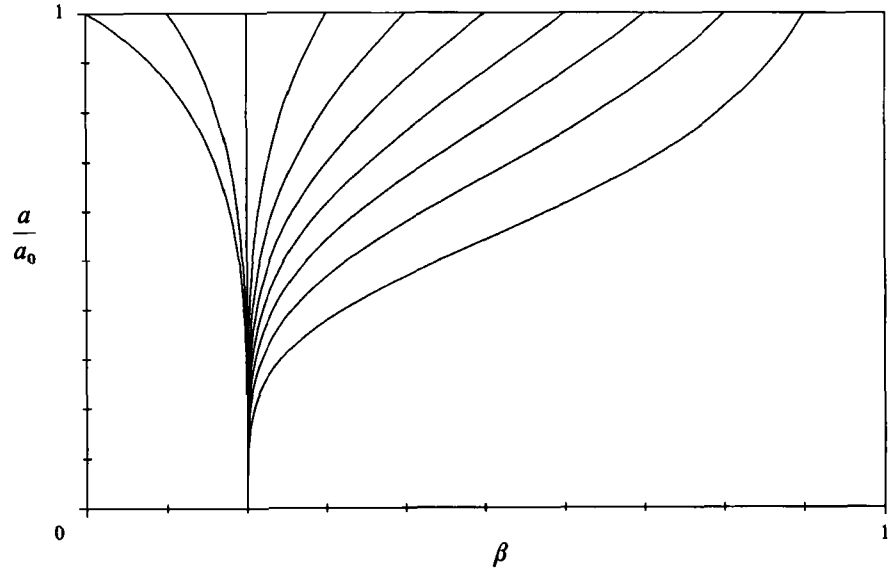

FIGURE 4. Dispersive term as a function of sound speed ratio across a centred unsteady expansion for different initial values of the dispersive term. $\gamma = \frac{7}{5}$. a_0 is the sound speed upstream of the expansion.

Figure 4 plots the dispersive term, β, as a function of the sound speed for different values of β_0 for a specific heat ratio of $\frac{7}{5}$. It can be seen that in the limit as the sound speed approaches zero β approaches $\frac{1}{2}(\gamma-1)$ independent of β_0. It could be said that the frequencies are 'focused' by the unsteady expansion. From (5.4) and (5.10), in the laboratory frame of reference, the focus frequency is

$$\nu = \frac{\lambda(a+\frac{1}{2}(\gamma-1)u)}{2\pi(1-(\frac{1}{4}(\gamma-1))^2)^{\frac{1}{2}}}. \tag{5.15}$$

From (4.1*a*) it can be seen that the bracketed term in the numerator of (5.15) is only dependent upon the steady-state conditions upstream of the expansion. Hence, if the conditions in the shock tube do not change, the frequency to which each mode is focused will be independent of the initial filling pressures and gases in the acceleration tube.

If all components of noise described by (5.3) were to traverse an unsteady expansion across which the sound speed dropped sufficiently, then at the downstream end of the expansion discrete narrow bands of frequencies corresponding to different modes should be observed. It is important to note that (5.15) implies that longitudinal waves ($\lambda = 0$) will not be observed as an oscillatory disturbance.

Focusing of the dispersive term across an unsteady expansion occurs because both the sound speed decreases and the gas velocity increases. If an interface is stationary with respect to the gas on either side and a decrease in the sound speed is the only physical quantity to change across the interface then from (5.4) the value of the dispersive term must increase. However, if a velocity increase is the only change across the interface then the equality (5.11) is preserved by a decrease in the value of the dispersive term (and therefore the fundamental frequency).

As a gas flows through an unsteady expansion the velocity increases and the sound speed decrease. Hence, two opposing changes to the value of the dispersive term will be produced by the expansion. It can be seen from (5.11) that the fundamental

frequency shift created by a velocity change is one which is multiplied by the dispersive term. Hence, if the dispersive term is small, the change in the velocity produces a less significant effect on the change to the value of the dispersive term than does the change in the sound speed. Hence, as the value of the dispersive term is driven by the change in sound speed, the value of the dispersive term increases. In contrast, if the dispersive term is sufficiently large that the velocity change drives the change in the value of the dispersive term then the dispersive term decreases. The net result is that the values of the dispersive term converge to one value.

5.2. *Amplitude change at an interface – reflection and transmission coefficients*

It will become apparent that the sound speeds on either side of the driver–test gas interface play a major role in determining the amplitude of the noise transmitted into the test gas. If the sound speed changes across an interface between two media then an acoustic wave approaching the interface will be both reflected and transmitted. If the interface is stationary relative to the two media the fundamental frequencies of the incident, reflected and transmitted waves are the same.

5.2.1. *Reflection on transmission coefficients for potential functions*

In the case of a longitudinal wave the reflection and transmission coefficients for the potential function ϕ are obtained by assuming the velocity and pressure are continuous across the interface. From (5.1) and (5.2) the reflection and transmission coefficients for the potential function ϕ are

$$C_{\mathrm{R}} = \frac{\beta_1 a_1 \gamma_2 - \beta_2 a_2 \gamma_1}{\beta_1 a_1 \gamma_2 + \beta_2 a_2 \gamma_1}, \tag{5.16}$$

and

$$C_{\mathrm{T}} = 2\frac{a_2}{a_1}\frac{\beta_1 a_2 \gamma_1}{\beta_1 a_1 \gamma_2 + \beta_2 a_2 \gamma_1}, \tag{5.17}$$

respectively, where β_1 and β_2 equal one and subscripts 1 and 2 refer to the medium in which the wave is incident and transmitted respectively. It should be noted that these coefficients are different to those for the velocity and pressure. These latter coefficients are determined from (5.16) and (5.17) via (5.1) and (5.2).

In the case of a lateral wave it can be seen from (5.1) that there are two non-zero velocity components. It is impossible to collectively satisfy continuity across the interface of both velocity components and the pressure. To overcome this dilemma and to be consistent with the no-penetration boundary condition (5.5) it will be assumed that slip can occur at the interface so that the axial velocity is the only component which is continuous across the interface. If the sound speed of the medium into which the wave is transmitted is less than ω/λ, so that β_2 is real, it can be shown as above that the reflection and transmission coefficients for the potential function ϕ are (5.16) and (5.17) respectively. However, if the sound speed of the medium into which the wave is transmitted is greater than ω/λ then β_2 is imaginary and exponential decay of the transmitted solution occurs. In this case the transmission coefficient (which determines the amplitude of the transmitted potential function at the interface) is

$$C_{\mathrm{T}} = 2\frac{a_2}{a_1}\frac{\beta_1 a_2 \gamma_1}{((\beta_1 a_1 \gamma_2)^2 - (\beta_2 a_2 \gamma_1)^2)^{\frac{1}{2}}}, \tag{5.18}$$

and the reflection coefficient is one.

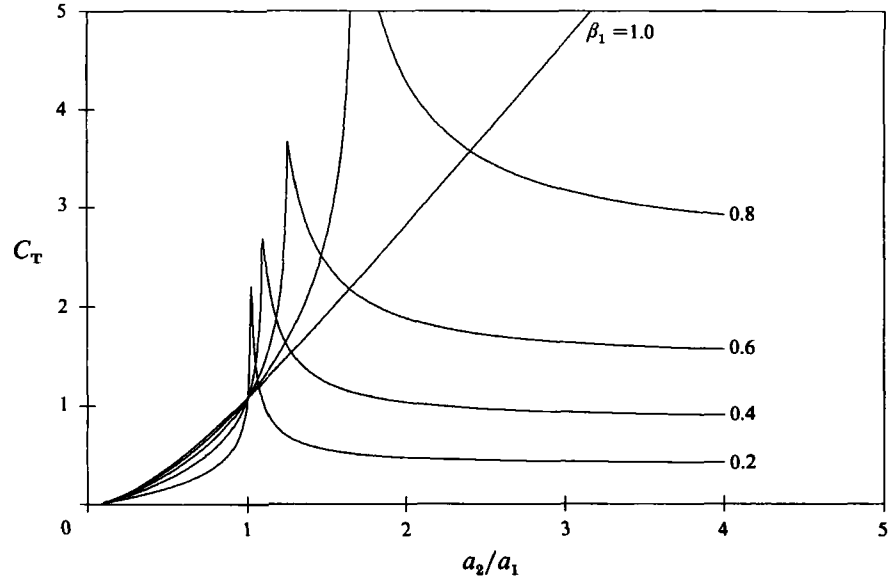

FIGURE 5. Transmission coefficients for different dispersive terms as a function of sound speed ratio across an interface. $\gamma_1 = \frac{5}{3}$. $\gamma_2 = \frac{7}{5}$.

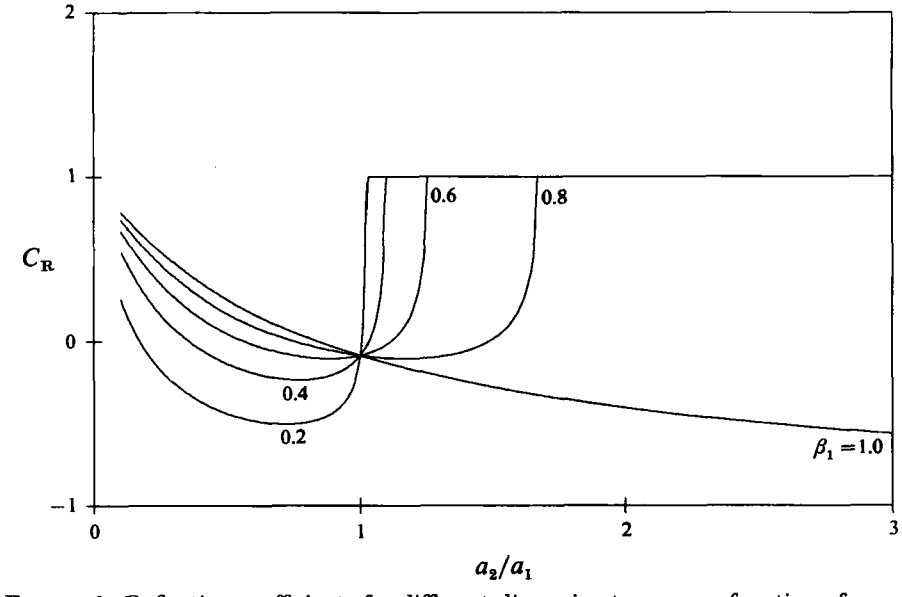

FIGURE 6. Reflection coefficients for different dispersive terms as a function of sound speed ratio across an interface. $\gamma_1 = \frac{5}{3}$. $\gamma_2 = \frac{7}{5}$.

5.2.2. *Minimum frequency transmitted across an interface*

Figures 5 and 6 show the transmission and reflection coefficients of the potential function as functions of sound speed ratio across the interface for different values of the incident wave dispersive term, $\gamma_1 = \frac{5}{3}$ and $\gamma_2 = \frac{7}{5}$. In figure 5 it can be seen that the transmission coefficient has a cusp for each value of the incident dispersive term. If the sound speed ratio is greater than that at the cusp the transmitted wave decays and the transmission coefficient is given by (5.18). For sound speed ratios less than

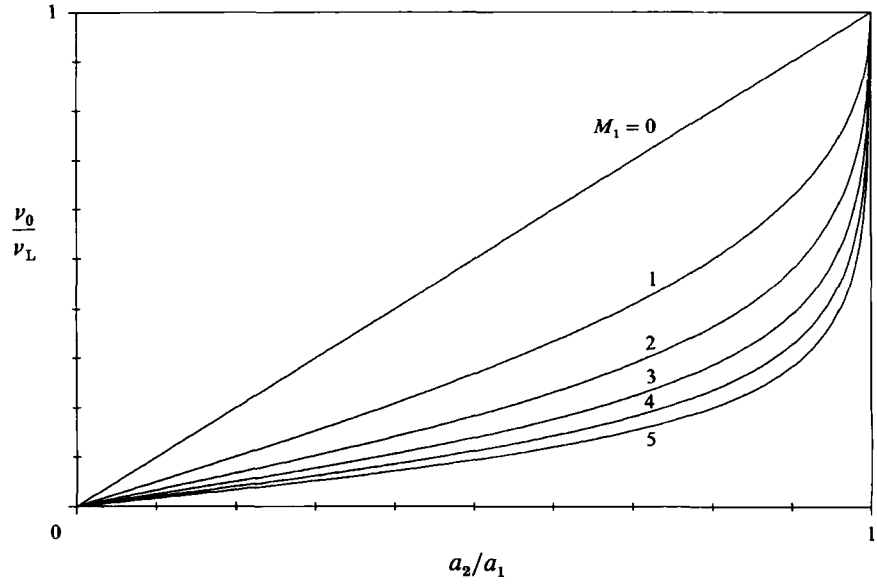

FIGURE 7. The ratio of the lowest possible lateral wave frequency to the lowest-frequency lateral wave which does not decay when transmitted, as a function of local sound speed ratio across the interface, for different values of the local Mach number of the incident region.

that at the cusp the transmitted wave does not decay and the transmission coefficient is given by (5.17). If the sound speed ratio is that for the cusp it can be seen from (5.1), (5.2) and (5.3) that the energy of the disturbance is totally confined in a pressure wave. The velocity of the disturbance is zero because β_2 is zero.

Remembering that β increases as ω increases, figure 5 indicates that for a given sound speed ratio, all frequencies above some minimum value will not decay. It is important to know this minimum frequency. Noting that it is the frequency for which β_2 equals zero, it follows from (5.4) that it occurs when ω equals λa_2. Recalling that the fundamental frequencies must match at the interface, the substitution of this value of the fundamental frequency into (5.4) gives the value of the corresponding incident dispersive term,

$$\beta_1 = (1-(a_1/a_2)^2)^{\frac{1}{2}}. \tag{5.19}$$

In an experiment the media move relative to the laboratory and by (5.10) this leads to an observed Doppler shift in frequency. If, in the incident medium, ν_L is the frequency measured in the laboratory frame of reference which corresponds to β_1 in (5.19), then from the substitution of (5.19) for β_1 in (5.10) and with the fundamental frequency determined from (5.4) it follows that

$$\nu_0/\nu_L = (a_1/a_2)\,(1 \mp M_1(1-(a_1/a_2)^2)^{\frac{1}{2}})^{-1}, \tag{5.20a, b}$$

where $M = u_1/a_1$ is the local Mach number of the medium in which the wave is incident, and

$$\nu_0 = \lambda a_1/(2\pi) \tag{5.21}$$

is the lowest frequency ($\beta = 0$) at which a lateral wave can exist in the incident medium. ν_L is the lowest frequency in the incident medium, as observed from a laboratory frame of reference, which would be transmitted through the interface.

Figure 7 displays the ratio ν_0/ν_L as a function of the shock speed ratio across the interface for different values of M_1 for waves travelling in the flow direction (5.20*b*).

In the experiments considered here the frequencies of the waves travelling upstream are too small to be considered as disruptive to the flow.

5.2.3. *Transmission coefficient for the Pitot pressure*

In §8 disturbances are in the main detected using centreline Pitot pressure measurements. Therefore, the transmission coefficient, C_{TP}, for the Pitot pressure perturbations is most relevant to the measurements presented below. Following convention, C_{TP} is defined as the ratio of the amplitude of the transmitted Pitot pressure perturbations to the amplitude of the incident Pitot pressure perturbations. This coefficient is determined in the normal way by first adjusting the amplitude of the potential function ϕ so that the amplitude of the incident Pitot pressure perturbation is unity. The transmission coefficient for ϕ given by (5.17) is then used in (5.8) to determine the amplitude of the transmitted Pitot pressure disturbances. It thus follows that this amplitude is the transmission coefficient for the Pitot pressure. When exponential decay does not occur it can be shown that

$$C_{TP} = \frac{\epsilon(M_2, a_2, \beta_2, \gamma_2)}{\epsilon(M_1, a_1, \beta_1, \gamma_1)} C_T. \tag{5.22}$$

6. Experimental determination of driver-gas properties and interface detection

The analysis of §8 requires the driver-gas sound speed to be determined immediately behind the driver–test gas interface. The location of the interface is also required. Two different methods are employed, depending on the physical quantities which were measured.

In some experiments the centreline Pitot pressure, static pressure and shock speed, U_s, were measured. In these cases Rayleigh's Pitot pressure formula (5.6) is used to determine the local Mach number of the driver gas. The driver-gas sound speed at the driver–test gas interface is obtained from this Mach number by assuming that the driver-gas velocity is equal to the test-gas velocity. The test-gas velocity is determined from real-gas calculations (McIntosh 1968, which is a modification of the code produced by Lordi, Mates & Moselle 1966) based on the measured shock speed. The accuracy of this technique is demonstrated in the Appendix where real-gas calculations of the test-gas Mach number are compared with the Mach number deduced from (5.6).

Where insufficient properties were measured to determine the Mach number from (5.6) the driver-gas sound speed at the driver–test gas interface is determined from the rupture pressure of the primary diaphragm, the sound speed and the filling pressure of the driver tube. It will be assumed that the mechanism through which the driver gas accelerates is as follows.

The driver gas is compressed adiabatically in the driver tube by the free piston until the primary diaphragm ruptures. At this time the driver gas is assumed to be at rest. The cross-sectional area of the driver tube is 7.3 times that of the shock tube. Therefore, to a good approximation, the driver gas in the driver tube remains at rest even after the primary diaphragm ruptures. It is assumed that the driver gas then undergoes a steady subsonic expansion to the entrance of the shock tube where the flow is assumed to be sonic. This point will be defined as the throat. From the throat the driver gas accelerates through an unsteady expansion to the velocity deduced

from the measured shock speed. In all calculations the driver gas is assumed to be perfect.

If P_0 and a_0 are the driver-gas pressure and sound speed before compression then the sound speed, a_1, when the primary diaphragm ruptures is given by

$$a_1 = a_0(P_1/P_0)^{\frac{\gamma-1}{2\gamma}}, \tag{6.1}$$

where P_1 is the primary diaphragm rupture pressure. This pressure was determined using a hydraulic rig. The pressure applied to a diaphragm is recorded as it is slowly increased. When the diaphragm ruptures the last recorded pressure is taken as the rupture pressure of the diaphragm.

For a large area ratio between the driver and shock tubes the sound speed at the throat, a_t, is approximately related to the sound speed before rupture by

$$a_t = \left(\frac{2}{\gamma+1}\right)^{\frac{1}{2}} a_1. \tag{6.2}$$

Finally, the driver-gas sound speed in the shock tube is related to the sound speed at the throat by (4.1a). Since the flow at the throat is sonic it then follows that

$$a_2 = \tfrac{1}{2}(\gamma+1)\,a_t - \tfrac{1}{2}(\gamma-1)\,u_2. \tag{6.3}$$

From (6.1), (6.2), (6.3) and real-gas calculations, which determine u_2 from the measured shock speed, the sound speed of the driver gas can be obtained.

The location of the interface has to be determined from Pitot pressure measurements. Since there is a change in Mach number across the interface there should, theoretically, be a change in the Pitot pressure at the interface. This is indeed observed; however, in addition, under certain conditions the mixing of the driver and test gases can produce a region of low-density gas at the interface (Levine 1970). This region would produce a dip in the Pitot pressure record. This characteristic is sometimes more distinguishable than the change in Pitot pressure created by the change in Mach number across the interface.

In §8 and the Appendix the interface is identified by first making a theoretical prediction using Mirels' (1964) analysis, then a dip and or a step change in the Pitot pressure is sought near this predicted location.

7. Test time limitations at high enthalpies

As outlined in §4 and displayed in figure 3, for sufficiently large acceleration-tube shock speeds, the test time is limited by the downstream edge of the unsteady expansion. If the conditions in the shock tube are unchanged and the acceleration tube shock speed is decreased then the test time should increase to its maximum. With a further decrease in acceleration-tube shock speed the test time should decrease as it is terminated by the reflection of the unsteady expansion off the driver–test gas interface. If the acceleration-tube shock speed is decreased sufficiently there will be no test time.

Figures 8(a)–8(d) are centreline Pitot pressure records which display these phenomena. The driver gas was argon. It was compressed from 120 kPa to the primary diaphragm rupture pressure of 34.5 MPa. The test and acceleration gases were air. The shock-tube filling pressure was 3.4 ± 0.15 kPa and the shock-tube shock speed was 2400 ± 200 m/s. The acceleration-tube filling pressure was varied between 5.4 ± 1 Pa and 66 ± 1 Pa which produced variation in acceleration-tube shock speed between 4400 m/s and 3700 m/s respectively.

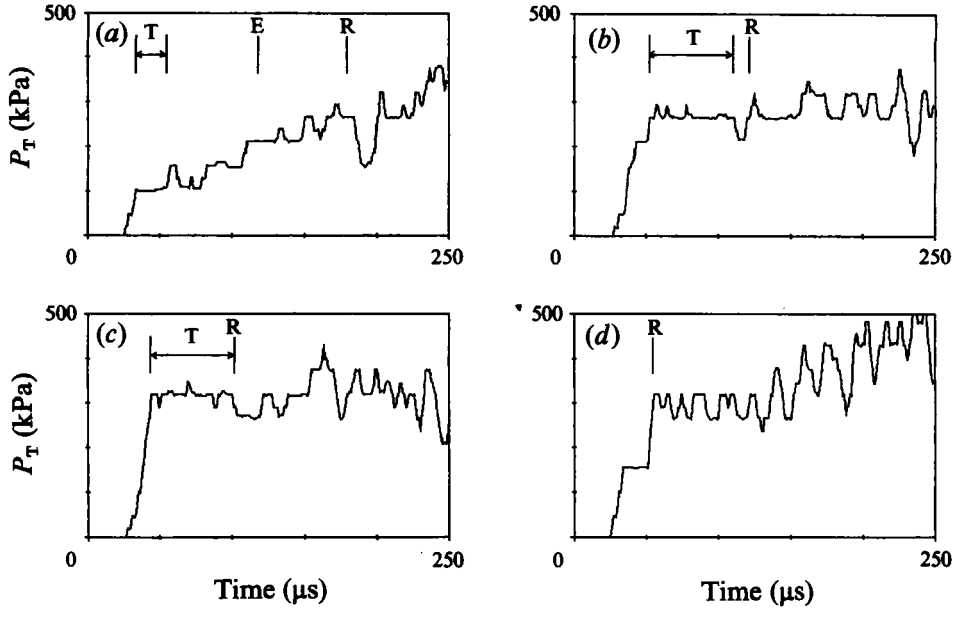

FIGURE 8. Expansion-tube centreline Pitot pressure records. Argon driver, air test and acceleration gases, $P_0 = 130$ kPa, $P_1 = 34.5$ MPa, $P_4 = 3.4$ kPa, $U_s = 2400$ m/s. T marks the test time, E marks the predicted downstream edge of the unsteady expansion and R marks the predicted downstream edge of the reflected unsteady expansion. (*a*) $P_7 = 5.4$ Pa, (*b*) $P_7 = 16$ Pa, (*c*) $P_7 = 26$ Pa, (*d*) $P_7 = 66$ Pa.

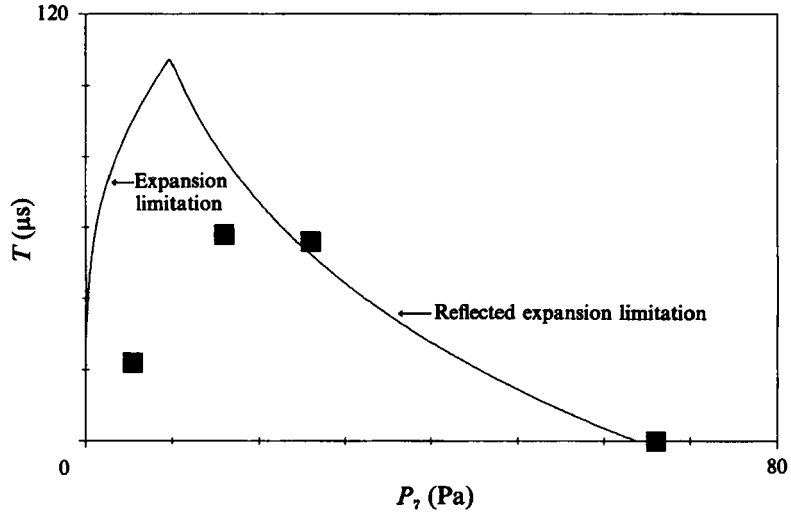

FIGURE 9. Test time as a function of acceleration-tube filling pressure. Air test and acceleration gases. Squares: Test time as measured from figure 8. $P_4 = 3.4$ kPa, $U_s = 2400$ m/s, $\gamma = \frac{7}{5}$, $r_0 = 18$ mm, $x_s = 3.18$ m, $x_A = 2.08$ m.

The theoretical locations of the downstream edge of the expansion (in figure 8*a*) and its reflection off the driver–test gas interface are marked with the letters E and R respectively. If the reflected expansion arrives before the expansion as in figures 8(*b*)–8(*c*) the location of the downstream edge of the expansion cannot be determined analytically and therefore is not located on these figures.

Figure 9 displays the predicted test time as a function of acceleration-tube filling pressure for the above shock-tube conditions. This figure also shows the measured values of the test time taken from figures 8(*a*)–8(*d*). It can be seen that there is reasonable agreement between prediction and measurement for the data at higher filling pressures.

In figure 8(*a*) the expansion limits the test time. The accuracy of the predicted test time in this case is not as good as in figures 8(*b*)–8(*d*) where it is limited by the reflected expansion. However, inspection of figure 9 indicates that when the test time is limited by the expansion, a small error in the acceleration-tube filling pressure will produce a large variation in the test time. Therefore this condition is not expected to produce accurate results.

8. Acoustic wave results

In this section experiments are presented which show that the oscillatory noise which is detrimental to the expansion tube test flow is consistent with a first-order lateral acoustic wave model. Furthermore, it is shown that a large proportion of this noise is generated in the driver gas in the region of the primary diaphragm.

8.1. *Shock-tube results*

Initially the secondary diaphragm was removed so that the expansion tube was simply a shock tube. This experiment was done to measure the spectral composition of the noise in the driver gas. These results are used in §8.2 to predict the attenuation of the noise which would occur in the expansion tube.

The driver gas was helium and was compressed from 130 kPa to 34.5 MPa at which point the primary diaphragm ruptured. The shock tube was filled with air to 2.66 kPa. The shock speed measured over the last 350 mm of the shock tube was 4000 m/s. Figures 10(*a*) and 10(*b*) respectively display the Pitot and static pressures as a function of time.

8.1.1. *Driver-gas flow properties*

Before a critical analysis of the spectral distribution of the driver-gas noise can be made the flow properties of the driver gas must be obtained over the period in which the spectral composition is obtained.

The location of the driver–test gas interface was determined as in §6 and is concluded to be coincident with the large dip in the Pitot pressure 43 μs after the shock. The spectral decomposition will be made in the relatively steady period between 200 and 456 μs after the shock. Within this period the Mach number and gas velocity are required.

The Mach number is obtained from Rayleigh's Pitot pressure formula, (5.6). The average Pitot and wall pressures in this period are 3780 and 720 kPa, respectively. Hence, from (5.6) with a specific heat ratio of $\frac{5}{3}$ the average local Mach number is 1.80.

The gas velocity is now determined from the shock speed. However, there is a complication. From figure 10(*b*) it can be seen that there exists a compression in the driver gas starting at the interface and extending to the start of the steady period over which the spectral decomposition is made. This disturbance is possibly caused by the acceleration of the driver–test gas interface. Whatever its cause may be, it will produce a difference between the velocity at the interface and the velocity during the period under consideration. In order to determine the velocity within this steady period it will be assumed that the sound speed and gas velocity can be related

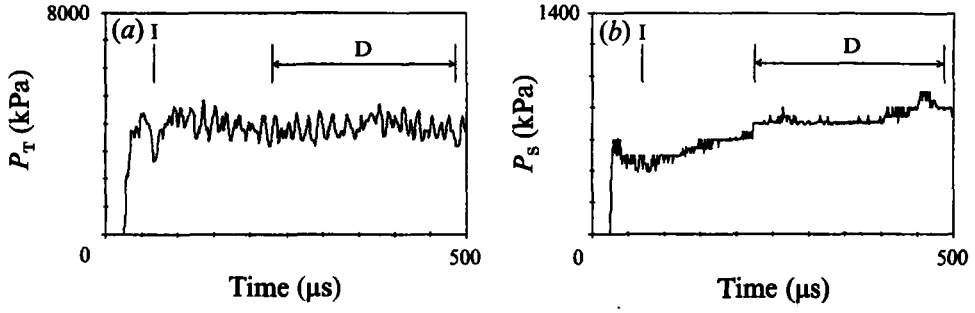

FIGURE 10. (*a*) Shock-tube centreline Pitot pressure and (*b*) static pressure records. Helium driver, air test and acceleration gases. *I* is the location of the interface. *D* is the period over which the decomposition was made. $P_0 = 130$ kPa, $P_1 = 34.5$ MPa, $U_s = 4000$ m/s, $P_4 = 2.66$ kPa.

throughout this disturbance by (4.1*a*). Hence, if the velocity and Mach number are known at the interface, then by (4.1*a*) and the Mach number just obtained, the gas velocity can be obtained.

Clear of the interface transients (80 μs after the shock) the unperturbed (or average) driver-gas Pitot and wall pressures are 4037 and 494 kPa, respectively. Hence, from (5.6) with $\gamma = \frac{5}{3}$ the unperturbed local Mach number of the driver gas at the interface is 2.29.

The driver-gas velocity at the interface is assumed to be equal to that of the test gas. Real-gas calculations based on the measured shock speed predict that the velocity of the test gas following the shock is 3600 m/s. It therefore follows that in the period between 200 and 456 μs after the shock, the unperturbed gas speed is 3120 m/s.

8.1.2. *Throat properties*

To establish that one of the primary sources for the noise is at the throat the driver-gas sound speed at the throat must be obtained. As outlined in §6 it can be obtained by two independent methods, either by using the driver-tube filling pressure and the primary-diaphragm rupture pressure or by using the gas velocity and sound speed at the interface.

The measured values of driver-tube filling pressure and the primary-diaphragm rupture pressure are 130 kPa and 34.5 MPa respectively. Hence, if the driver-gas sound speed before compression is assumed to be 1008 m/s then from (6.1) and (6.2) the driver-gas sound speed at the throat should be 2665 m/s. However, the gas speed and Mach number at the interface are 3600 m/s and 2.29, respectively, hence, by (6.3) the sound speed at the throat is required to be 2079 m/s.

The source of this discrepancy is not known; however, it is conceivable that the compression in the free piston driver is non-adiabatic. It is also possible that the static method which was used to determine the rupture pressure of the primary diaphragm may produce a different rupture pressure to that which actually occurs when the diaphragm is ruptured dynamically, as in the free piston facility. Notwithstanding this discrepancy it will be assumed that the value deduced from the shock speed measurement, 2080 m/s, is the better estimate of the sound speed at the throat.

8.1.3. *Noise spectral decomposition*

A spectral decomposition of the driver-gas noise measured along the centreline by the

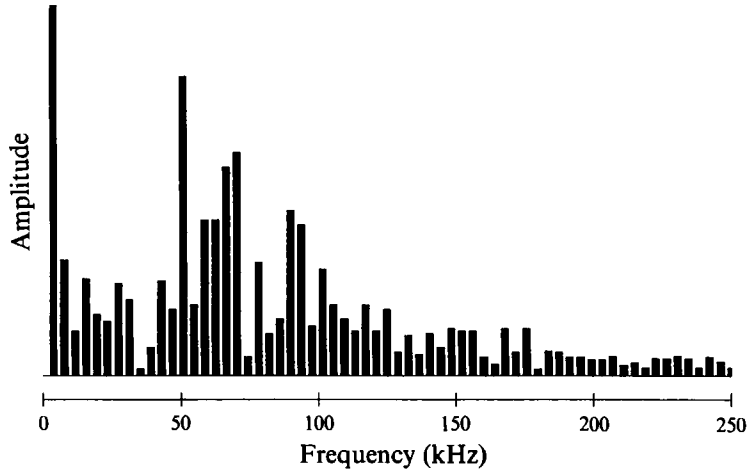

FIGURE 11. Spectral decomposition of Pitot record of figure 10(*a*) between 200 and 456 μs after shock.

Pitot probe was made. Figure 11 displays the composition of the Pitot pressure signal over the time period between 200 and 456 μs after the arrival of the shock. This region was chosen as the unperturbed wall pressure is reasonably steady. It can be seen that the spectrum has maxima in the ranges 0–5, 50–70 and 74–120 kHz. The noise detrimental to the flow quality lies in the frequency range at and above 50 kHz.

From the flow properties deduced in the previous section it can be shown from (5.4) and (5.10) with $\beta = 0$ that first-order lateral waves exist at frequencies greater than 55 kHz. Thus, it is possible for the majority of the detrimental noise to be first-order lateral waves.

8.1.4. *Noise source*

The origin of the noise is also of interest. One obvious source of noise is the primary-diaphragm rupturing process. If acoustic waves generated at the throat are transmitted through the unsteady expansion centred at this diaphragm then, as shown in §5.1.2, every frequency of each acoustic wave mode would approach the frequency (5.15), where λ is determined by the mode. Hence, for a gas speed of 3120 m/s and a Mach number of 1.8 the first-order lateral waves should approach 94.2 kHz.

However, the focusing effect of the unsteady expansion centred at the throat is weak because the sound speed ratio across the expansion is only 0.83. Furthermore, for a monatomic gas, the power to which this ratio is raised in (5.14) is two. Therefore, rather than a distinct frequency, a band of frequencies distributed about the focus frequency would be expected after the unsteady expansion.

If the lowest-frequency first-order lateral wave ($\beta = 0$) was excited at the throat then downstream of the expansion this component can be shown from (5.4) and (5.10) to have a frequency of 70 kHz. This would be the lowest frequency in the band.

It can be seen in figure 11 that the 74–120 kHz range has a definite peak between 90 and 94 kHz which would be consistent with weak focusing of first-order lateral waves originating at the throat. Furthermore, the lowest frequency of this range is also consistent with being produced at the throat. Hence, it is concluded that this part of the spectrum consists of first-order lateral waves which in the main originate at the throat.

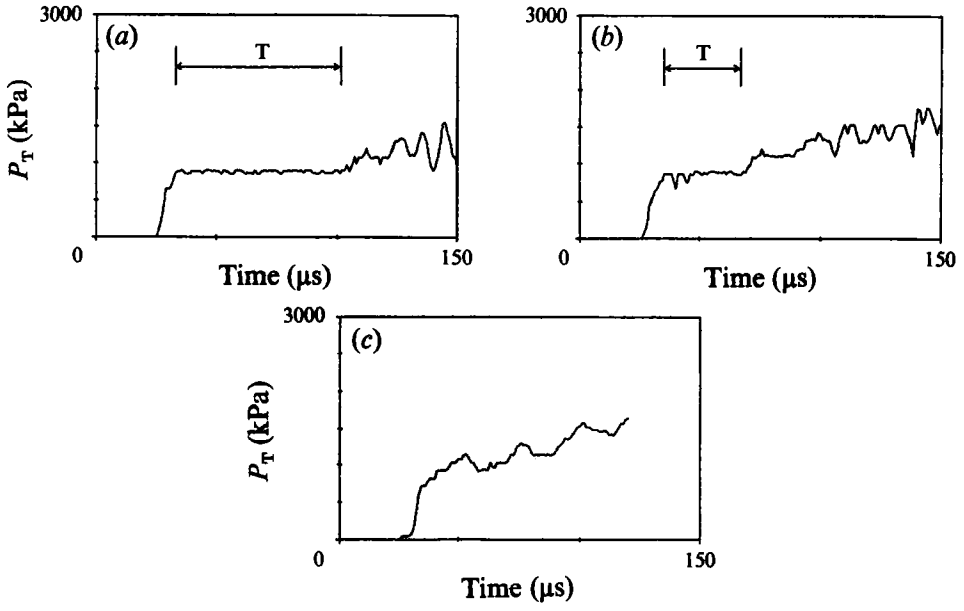

FIGURE 12. Expansion-tube centreline Pitot pressure measurements. Helium driver, air test and acceleration gases. T marks the test time. $P_0 = 130$ kPa. $P_1 = 34.5$ MPa. See table 1 for flow properties of (*a*), (*b*) and (*c*).

Figure	U_s (m/s)	U_3 (m/s)	a_2 (m/s)	a_3 (m/s)	U_{ss} (m/s)	P_4 (kPa)	P_7 (Pa)
12(*a*)	5270	4814	1164	1588	9200	3.46	16
12(*b*)	4800	4325	1327	1572	8970	6.65	17
12(*c*)	3650	3291	1672	1138	7640	13.2	16

TABLE 1. Flow properties of the driver and test gas either side of the driver–test gas interface for figure 12. Numbered subscripts refer to the regions defined in figure 2.

The origin of the 50–70 kHz components is not known. However, it will be seen in the next section that in the experiments reported here they do not govern the bounds for acceptable test conditions.

8.2. *Expansion-tube results*

In §5.2 it was seen that a lateral wave incident upon the driver–test gas interface will be attenuated in the test gas if the sound speed of the driver gas is sufficiently less than that of the test gas. Owing to the relatively short test-gas slug length it is difficult to see from shock-tube Pitot pressure results whether or not the noise observed in the driver gas is transmitted into the test gas. However, the effect of the interface can be seen in expansion-tube results where the test-gas slug has been expanded.

8.2.1. *Helium-driven expansion tube*

Figure 12 displays the expansion-tube centreline Pitot pressure records for different shock-tube filling pressures when a helium driver was used. The driver conditions are the same as in §8.1. Table 1 tabulates the driver- and test-gas flow properties in the shock tube either side of the driver–test gas interface. These conditions were chosen so that driver-gas sound speed ranged from being less than to greater than that of the test gas.

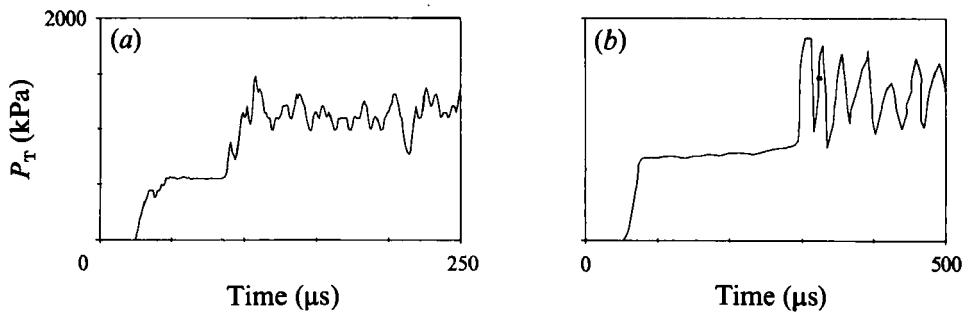

FIGURE 13. Expansion-tube centreline Pitot pressure measurements displaying the effect of the test–acceleration gas interface on the noise in two different facilities. (*a*) Present experiment, (*b*) a reproduction of Norfleet *et al.* (1965, figure 26).

In table 1 the test-gas velocity and sound speed were obtained from real-gas calculations based on the measured shock speed. The test-gas velocity was assumed to be equal to the driver-gas velocity at the interface. The driver-gas sound speed was then determined from (6.3) where the throat sound speed was assumed to be 2080 m/s.

From figure 7, for a driver-gas Mach number of approximately three, the test-gas Mach number need only be 2% less to attenuate frequencies twice as high as the lowest-frequency lateral wave ν_0. Hence, from figure 11, as $\nu_0 = 55$ kHz, a 2% increase in sound speed would attenuate the majority of the noise produced in the driver gas.

From table 1 it can be seen that the driver-gas sound speed is less than the test-gas sound speed at the two higher shock speeds (figures 12*a* and 12*b*) and the reverse situation occurs at the smallest shock speed (figure 12*c*). There is a 36% and 18% increase in sound speed across the driver–test gas interface for the conditions which produced figures 12(*a*) and 12(*b*) respectively. Hence, only minimal noise should be transmitted into the test gas. This is indeed displayed in these figures. Furthermore, it can be seen in figure 12(*c*), where the test-gas sound speed is less than the driver-gas sound speed, that significant noise disrupts the flow. Thus, these results are consistent with the assertion that the disturbances are first-order lateral waves which are generated in the driver gas.

8.2.2. *Test–acceleration gas interface*

A significant result which confirms the existence of lateral waves and the non-existence of longitudinal waves in the test gas is displayed in figures 13(*a*) and 13(*b*). These figures are the centreline Pitot pressure record from different expansion tubes, both of which used air test and acceleration gases. Figure 13(*a*) is the centreline Pitot pressure in the expansion tube described in §3, which has an internal diameter of 37 mm. Figure 13(*b*) is the centreline Pitot pressure obtained by Norfleet *et al.* (1965) from an expansion tube with an internal diameter of 102 mm.

From figure 2 it can be seen that the acceleration gas which arrives at the test section before the test gas would, in general, have a different sound speed to that of the test gas. The steps in figures 13(*a*) and 13(*b*) are produced because of this difference in sound speed. To the right of the step is the test gas and to the left is the acceleration gas. In figure 13(*a*) the Pitot pressure measured in the acceleration gas is approximately half that in the test gas. Hence, the acceleration gas sound speed is approximately $\sqrt{2}$ that of the test gas. Therefore, as the acceleration-gas sound speed is greater than the test-gas sound speed the interface will act as a filter to

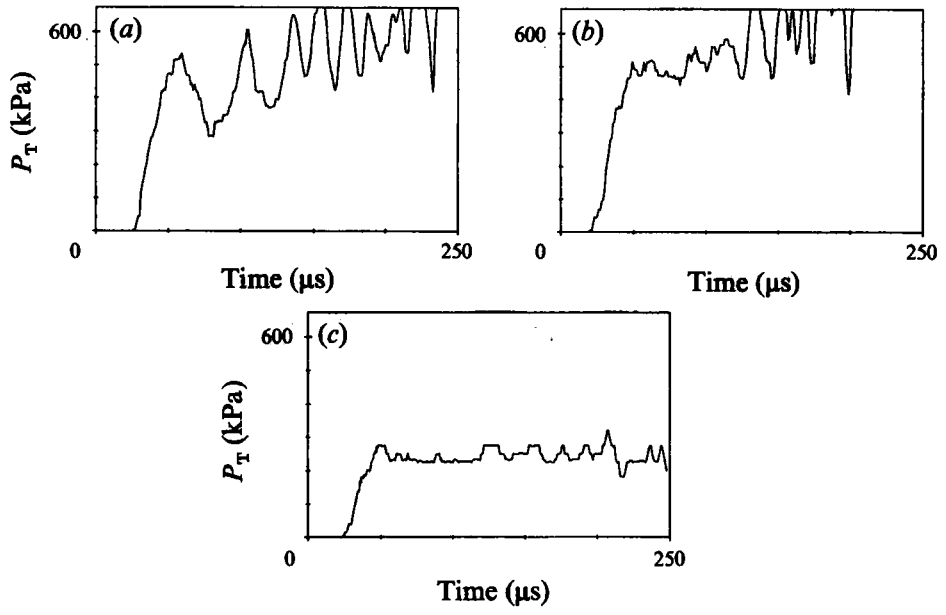

FIGURE 14. Expansion-tube centreline Pitot pressure measurements. Argon driver gas, air test and acceleration gases. $P_1 = 34.5$ MPa. See table 2 for flow properties of (*a*), (*b*) and (*c*).

Figure	U_s (m/s)	U_3 (m/s)	a_2 (m/s)	a_3 (m/s)	P_0 (kPa)	P_4 (kPa)	P_7 (Pa)
14(*a*)	2050	1714	621	866	125	13.7	17
14(*b*)	2000	1668	618	851	130	13.7	32
14(*c*)	2350	1995	526	941	120	3.46	33

TABLE 2. Flow properties of the driver and test gases either side of the driver–test gas interface for figure 14. Numbered subscripts refer to the regions defined in figure 2

lateral waves. From the measured shock speed of 3700 m/s and (5.20*b*) it can be shown that $\nu_0/\nu_L \approx 0.2$, hence, a significant band of lateral wave frequencies will be attenuated.

In contrast, from (5.17) and (5.22) the transmission coefficient for a longitudinal wave would be approximately 0.8. Thus, only a slight decrease in the relative size of the disturbance to the unperturbed state should be observed if the disturbance is a longitudinal wave.

It is observed in figure 13(*a*, *b*) that effectively no disturbances are transmitted into the acceleration gas in either facility. Thus, this disturbance is consistent with the lateral wave model and furthermore is inconsistent with the longitudinal wave model.

8.2.3. *Argon-driven expansion tube*

In §8.2.1. helium was used as a driver gas. As a result the sound speed of the driver gas was relatively high at the throat. In this section expansion-tube experiments are presented for an argon driver gas to display the effect that drivers with lower sound speed have on noise transmitted through the driver–test gas interface.

Figure 14(*a–c*) shows centreline Pitot pressure records from an expansion tube when the test gas was driven by argon. Table 2 tabulates the properties of the driver and test gases. Owing to the lack of shock-tube Pitot pressure measurements the

driver-gas properties were obtained assuming the driver gas was adiabatically compressed in the driver tube, as outlined in §6.

The value of ν_L/ν_0 for the driver–test gas interface determined from (5.20*b*) and table 2 is 3.9 compared with 3.23 for the helium driver used for figure 12. Hence, a slightly more favourable ratio exists for the argon driver and yet there is significantly more noise in the test gas. This apparent paradox occurs because the argon-driver-gas sound speed is about one third of the helium-driver-gas sound speed. Hence, from (5.21) the highest frequency which is attenuated at this interface is approximately one third of the highest frequency which is attenuated across the helium-driver–test gas interface. Therefore, the higher frequencies associated with diaphragm rupture are not completely attenuated. This shows that the driver-gas sound speed at the time when the primary diaphragm ruptures is important in determining the magnitude of the increase in the sound speed across the driver–test gas interface.

In the above argument it is assumed that the band of frequencies which are incident upon the driver–test gas interface for the argon driver is the same as that for the helium driver. This is not strictly correct. It should be understood that different driver-gas sound speeds at the throat will produce different ranges of frequencies incident upon the driver–test gas interface. This change in bandwidth is relatively minor in the experiments reported here; however, for completeness the band of frequencies originating in the argon driver gas which is incident upon the driver–test gas interface will be determined.

It is assumed that the frequencies relative to the laboratory produced when the primary diaphragm ruptures are functions of tunnel and diaphragm geometry. Thus, provided these geometries remain the same, the band of frequencies relative to the tunnel which are induced into the driver gas is identical at the throat for all driver-gas sound speeds. However, since the Doppler effect on lateral waves is dependent on sound and gas speed and not simply Mach-number dependent the fundamental frequencies induced into the driver gas at the throat will depend on the sound speed at the throat. This in turn produces a different range of frequencies which will be incident on the driver–test gas interface.

It is assumed that the frequency range 74–125 kHz with a peak at 92 kHz in figure 11 is produced by the primary diaphragm. Following the above assumptions, for figure 14(*b*), the primary diaphragm would produce a band of frequencies from 67–117 kHz with a peak at 85 kHz in the shock tube at the driver–test gas interface. The lowest unattenuated frequency determined from (5.20*b*) for this condition is 78 kHz. Hence, it can be seen that only a portion of the diaphragm noise, which does not include the peak, would be attenuated under these circumstances.

Figure 14(*c*) was produced by increasing the shock speed in the shock tube by lowering the shock-tube filling pressure. There was also a minor change in the driver-gas filling pressure. The overall effect is to dramatically increase the highest attenuated frequency. For this condition the primary diaphragm would produce a band of frequencies in the driver gas from 63–107 kHz with a peak at 78 kHz. The lowest unattenuated frequency determined from (5.20*b*) is 133 kHz. Hence, it can be seen that all the noise would be attenuated at the driver–test gas interface. This is reflected in the experimental results.

8.2.4. *Resonance in an expansion tube*

An interesting phenomenon occurs in figure 14(*a*). From table 2 it would appear that the shock-tube conditions for both figures 14(*a*) and 14(*b*) are almost identical and yet a vastly different result occurs. The acceleration-tube filling pressures were

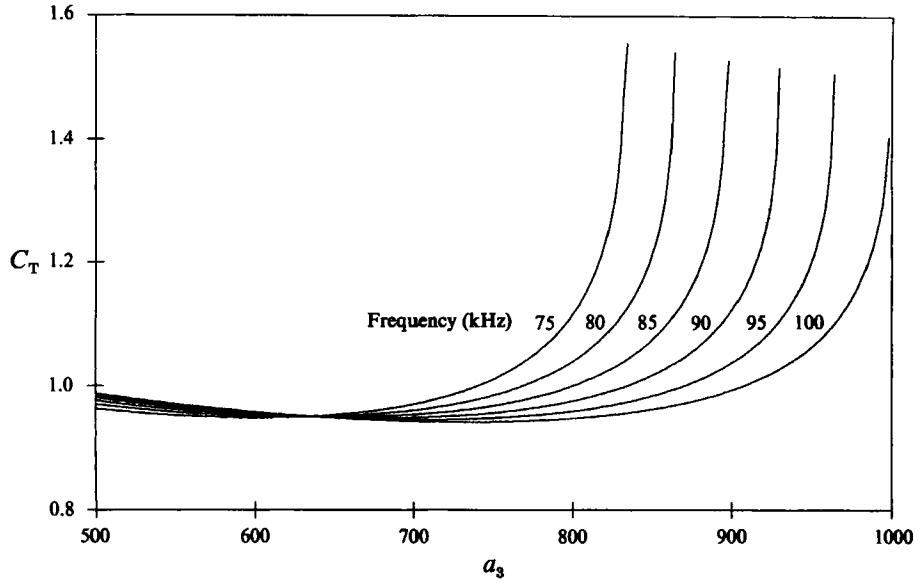

FIGURE 15. Pitot pressure transmission coefficient as a function of test-gas sound speed at different frequencies, for disturbances transmitted from the driver gas to the test gas. Driver-gas conditions are as listed in table 2, figure 14(*b*). Frequencies are measured from a laboratory frame of reference and are the frequencies of the disturbance in the driver gas. $\gamma_2 = \frac{5}{3}$, $\gamma_3 = \frac{7}{5}$.

different in the two cases, but it is not believed that this is the cause of the amplification, or resonance, of the noise.

Figure 15 displays the Pitot pressure transmission coefficient (5.22) of first-order lateral waves as a function of test-gas sound speed. The driver conditions are those given in table 2 for figure 14(*a*). These transmission coefficients are for disturbances transmitted downstream from the driver gas into the test gas. It can be seen that the transmission coefficient is dependent upon the frequency of the disturbance. The frequencies displayed in figure 15 are those of disturbances in the driver gas measured from a laboratory frame of reference.

There are two important features displayed in figure 15. First, it can be seen that if the test-gas sound speed is increased beyond that the driver-gas sound speed (621 m/s) then the transmission coefficient becomes increasingly dependent upon the frequency of the disturbance in the driver gas. Secondly, it can be seen that as the test-gas sound speed increases, the transmission coefficient asymptotes to a finite value. If the sound speed is increased beyond this point, exponential decay of the transmitted disturbance occurs.

Close to the asymptote, it can be seen that only a small change in the test-gas sound speed results in a sizable change in the transmission coefficient. Therefore, if the change in sound speed across the driver–test gas interface is such that the predominant frequency of the disturbance in the driver gas is close to the lowest unattenuated frequency, then a very unstable situation occurs where only a slight change in the conditions will produce a large change in the amplitude of the noise transmitted into the test gas.

It is interesting to note that for figure 14(*a*) the primary diaphragm would produce a band of frequencies in the range 68–118 kHz with a peak at 86 kHz. The lowest unattenuated frequency is 82 kHz. Hence, the peak frequency is close to the lowest unattenuated frequency, as is also the case in figure 14(*b*). It is therefore conceivable

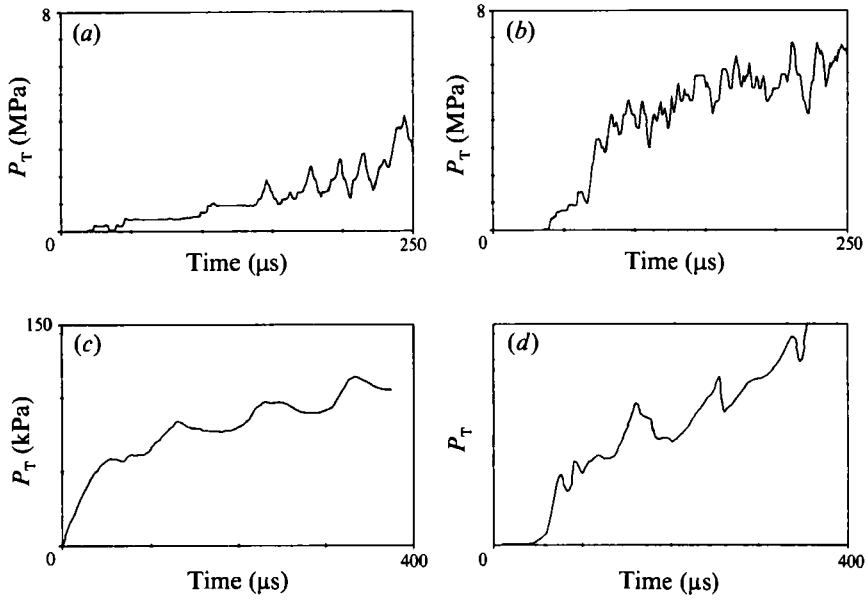

FIGURE 16. Expansion-tube centreline Pitot pressure measurements. Air test and acceleration gases; $r_0 = 0.018$ m: (*a*) $U_s = 2410$ m/s, $U_{ss} = 5970$ m/s, $a_3/a_5 = 0.46$, (*b*) $U_s = 2500$ m/s. $U_{ss} = 4680$ m/s, $a_3/a_5 = 0.67$. (*c*, *d*) Pitot pressure records obtained by Miller (1977) and Norfleet *et al.* (1965) respectively.

that the radically different amplification of the noise in figures 14(*a*) and 14(*b*) results from the closeness of the unattenuated frequency to the frequency at which the driver-gas noise produce by the primary diaphragm peaks.

9. Frequency focusing

In §5.1.2 it was shown that, provided a significant drop in the sound speed occurred across an unsteady expansion, the different components of the noise upstream of the expansion would be focused to one particular frequency for every different mode. Furthermore, from figure 4 it can be seen that the degree of focusing is very sensitive to the ratio of sound speeds across the expansion. For a specific heat ratio of $\frac{7}{5}$ focusing becomes significantly more pronounced for sound speed ratios of less than 0.5.

The degree to which noise is focused by different sound speed ratios across the unsteady expansion centred at the secondary diaphragm in an expansion tube has been observed using centreline Pitot pressure measurements. Different sound speed ratios across this expansion were obtained by changing the acceleration-tube filling pressure. Conditions upstream of the expansion were not changed. Pitot pressure measurements are shown in figures 16(*a*) and 16(*b*) where the sound speed ratios across the unsteady expansion were 0.46 and 0.67 respectively. These values were derived from the sound speed in the shock tube assuming the gas is perfect with $\gamma = \frac{7}{5}$.

From figure 4 it can be seen that significantly more focusing should occur at the lower sound speed ratio. This is reflected in the experimental results. In figure 16(*a*) it can be seen that a structured disturbance does occur downstream of the expansion, where as in figure 16(*b*) the disturbance is less structured. If the shock speed prior to

secondary-diaphragm rupture is used to predict the values of u and a upstream of the expansion then from (5.15), for a perfect gas with $\gamma = \frac{7}{5}$, the period corresponding to a fully focused first-order lateral wave is 21 μs. Real-gas calculations which assume the flow is frozen within the expansion predict a more strongly focused disturbance, due to the decrease in specific heat ratio, with a period of 25 μs. The measured value taken between 170 and 220 μs in figure 16(*a*) is 21 ± 2 μs.

The effect of focusing has also been observed in the facilities used by Miller (1977) and Norfleet *et al.* (1965). The inside diameters of these facilities are 152 and 102 mm respectively, which are significantly different to the inside diameter of the facility which produced figure 16(*a*) (37 mm). Figures 16(*c*) and 16(*d*) are the Pitot pressure records obtained by Miller (figure 6) and Norfleet *et al.* (figure 25), respectively. For a fully focused first-order lateral wave the period of the disturbance in Miller's experiment should be 104 μs and in Norfleet *et al.*'s experiment it should be 69 μs. This compares satisfactorily with the measured values of approximately 100 μs, average of the period between 130 and 330 μs in figure 16(*c*), and 89 μs average over the period between 160 and 340 μs in figure 16(*d*), respectively.

Remembering that longitudinal waves would not produce such an oscillatory disturbance, these experimental results can be accepted as evidence that lateral acoustic waves are the dominant mode of the flow disturbances.

10. Conclusions

It has been shown that the test time in an expansion tube can be limited by either the wave system associated with the unsteady expansion centred at the secondary diaphragm or by disturbances in the driver gas. These disturbances can be modelled as first-order lateral waves.

The wave system may limit the test time through arrival at the test section of either the downstream edge of the unsteady expansion, or the downstream edge of the reflection of the upstream edge of this expansion from the driver–test gas interface. The maximum test time occurs when the two arrive simultaneously, a condition which is sensitive to the length of the acceleration tube, as well as to the velocity ratio across the expansion. This sensitivity is such that a variable acceleration-tube length is likely to be an important feature of a practical expansion-tube facility.

The acoustic waves in the driver gas limit the test time by penetrating the driver–test gas interface, and ultimately appearing as flow disturbances in the expanded test gas. Their existence as lateral acoustic waves was established through experimental confirmation of an analysis which predicted that focusing of these waves towards a particular frequency would occur when the test gas was subjected to a strong unsteady expansion. The effect would not be observed for longitudinal acoustic waves.

The penetration of these waves into the test gas can be inhibited by choosing driver conditions such that there is sufficient increase in the speed of sound from the expanded driver gas to the test gas at the driver–test gas interface. The magnitude of the required increase grows with the frequency of the waves to be inhibited and reduces as the driver-gas sound speed increases. These features signify that, unless some means of elimination of the lateral acoustic waves in the driver gas can be found, expansion tubes can only be expected to operate successfully when the Mach number of the driver gas at the interface exceeds certain critical values. Values of 4 to 5 were suggested by the experiments reported here, indicating that substantial

driver-gas expansion ratios may be required, and when this is combined with the advantage conferred by a high driver-gas sound speed it implies that an expansion tube may be most useful towards the high velocity end of its theoretical range of operation.

The authors wish to acknowledge the financial support received through NASA Langley Research Center, Grant No. NAGW 674. The authors also wish to acknowledge C. Gourlay for his insight in recognizing the significance of the reflection of the unsteady expansion off the driver–test gas interface and I. Stringer for his assistance in the experiments.

Appendix. Validation of Mach number predictions

To predict the attenuation of the noise transmitted into the test gas it is essential to know the Mach numbers and velocities of both test and driver gases. The Mach number of the test gas is obtained from real-gas calculations based on shock speed and shock-tube filling pressure; however, the Mach number of the driver gas must be determined from Pitot and static pressure measurements using Rayleigh's Pitot pressure formula (5.6). The accuracy of this method is established by comparing the real-gas predicted Mach number with that determined from the static and Pitot pressure measurements made in the test gas in the shock-tube experiment described in §8.1.

Real-gas calculations predict that the velocity of the test gas following the shock is 3600 m/s, the Mach number is 2.7, the static pressure is 450 kPa and the equilibrium specific heat ratio is 1.22. The location of the driver–test gas interface was determined as in §6 and is concluded to be coincident with the large dip in the Pitot pressure 43 μs after the shock. The Pitot and static pressures measured between 14 and 40 μs after the shock are 4133 ± 300 and 473 ± 30 kPa respectively. Using these measured pressures and a specific heat ratio of 1.22, Rayleigh's Pitot pressure formula (5.6) predicts a Mach number of 2.66 ± 0.18, which is in good agreement with the theoretical value of 2.7.

REFERENCES

GODUNOV, S. K. 1959 A difference method for numerical calculation of discontinues solutions of the equation of hydrodynamics. *Mat. Sb.* **47**, 271–306.

LEVINE, M. A. 1970 Turbulent mixing at the contact surface in a driven shock wave. *Phys. Fluids* **13**, 116–117.

LIEPMANN, H. W. & ROSHKO, A. 1957 *Elements of Gas Dynamics*. Wiley.

LORDI, J. A., MATES, R. E. & MOSELLE, J. R. 1966 Computer program for numerical solution of nonequilibrium expansions of reacting gas mixtures. *NASA CR*-472.

MCINTOSH, M. K. 1968 Computer program for the numerical calculation of frozen and equilibrium conditions in shock tunnels. Dept. of Physics, ANU Canberra.

MILLER, C. G. 1977 Operational experience in the Langley expansion tube with various test gases. *NASA Tech. Mem.* 78637.

MIRELS, H. 1964 Shock tube test time limitation due to turbulent-wall boundary layer. *AIAA J.* **2**, 84–93.

NEELY, A. J., STALKER, R. J. & PAULL, A. 1991 High enthalpy, hypervelocity flows of air and argon in an expansion tube. *Aeronaut. J.*

NORFLEET, G. D., LACEY, J. J. & WHITFIELD, J. D. 1965 Results of an experimental investigation of the performance of an expansion tube. In *Fourth Hypervelocity Tech. Symp., AEDC Tullahoma, Tennessee, Nov.*, pp. 49–110.

PAULL, A. & STALKER, R. J. 1991 The effect on an acoustic wave as it traverses an unsteady expansion. *Phys. Fluids* A **3**, 717–719.

SPURK, J. H. 1965 Design, operation, and preliminary results of the BRL expansion tube. In *Fourth Hypervelocity Tech. Symp., A.E.D.C. Tullahoma, Tennessee, Nov.*, pp. 111–144.

STALKER, R. J. 1966 The free piston shock tunnel. *Aeronaut. Q.* **17**, 351–370.

TRIMPI, R. L. 1962 A preliminary theoretical study of the expansion tube, a new device for producing high-enthalpy short-duration hypersonic gas flows. *NASA TR* R-133.

WHITHAM, G. B. 1974 *Linear and Nonlinear waves*. Wiley.